CrossMark

Enhanced sensitivity and response speed of graphene oxide/ZnO nanorods photodetector fabricated by introducing graphene oxide in seed layer

Sisi Liu[1] · Bo Li[1] · Hao Kan[1] · Ming-Yu Li[1] · Bing Xie[1] · Shenglin Jiang[1] · Xiao Zhu[1]

Abstract Graphene/ZnO nanocomposites photodetectors hold great potential for UV detection because of the combination of photosensitive ZnO and high electron-mobility graphene. In this paper, graphene oxide (GO)/ZnO nanorods photoconductive photodetector with seed layer of GO and ZnO nanocrystals (NCs) hybrids is fabricated via a low-cost solution process. Uniform and oriented GO/ZnO nanorods have been obtained due to the positive role of GO in the growth process of ZnO nanorods, which gives rise to less light scattering and thereby stronger absorption and enhanced photocurrent. When the growth time is 1 h, the optimum photocurrent of GO/ZnO nanorods is about 9.4 times than pure ZnO nanorods, meanwhile, the corresponding detectivity reaches 7.17×10^{11} cm $Hz^{1/2}$ W^{-1}. In addition, owing to the high carrier mobility of graphene, the response time t_{90} of GO/ZnO photodetector beneficially decreases to ~1 s, which is much faster than many other GO/ZnO hybrid photodetectors.

1 Introduction

Semiconductor nanostructures, such as nanoparticles (NPs), quantum dots (QDs), nanowires (NWs) or nanorods (NRs), have been widely researched for the potential application in photodetectors, light-emitting diodes, thermo-electric devices, photocatalysts etc [1–5]. Regarding UV light detection, Zinc oxide (ZnO) is an adequate material in UV–Visible spectral region because of its wide band gap of 3.37 eV and high excitation binding energy of 60 meV at room temperature [6, 7]. One-dimensional (1D) ZnO nanostructures such as nanorods and nanowires are more suitable for fabricating high sensitive UV photodetector as a result of its large surface area and high carrier mobility [8, 9]. Graphene is a novel carbon nanomaterial with unique two dimensional (2D) conjugated structure, possessing superior mobility of charge carriers at room temperature (200,000 cm^2 V^{-1} S^{-1}) and excellent transparency (~97.7%) [10–14], thus, it has been widely studied for applications in optoelectronic devices and various sensors [15–17]. However, the weak light absorption and zero band gap of graphene results in a poor response for light with the low photoresponsivities between 0.1 and 0.5 mA W^{-1} [18], which in turn limit its applications in photodetectors. Fortunately, the photoelectronic properties of graphene can be greatly improved by forming composites with semiconductor nanomaterials [19–22]. Recently, graphene/1D ZnO hybrids structures have received enormous attention owing to the combination of the superior light absorption of ZnO and the fast charge mobility of graphene, both of which are critical to applications of UV photodetector. The photocurrent of graphene/ZnO nanowire photodetector can reach 65 µA, however, the relatively high dark current of ~45 µA resulted in a low switch ratio and high noise [23]. The photoresponsivity of ZnO nanorod/graphene heterostructure photodetector have reached 22.7 A W^{-1}, which was over 45000 folds higher than that of single graphene sheet based photodetector, but, the response requires a longer time over 350 s [17]. Therefore, it is still a challenge to prepare excellent photodetector with high photoresponse, switch ratio, detectivity and fast response and recovery time.

The most primary approaches to prepare 1D ZnO nanomaterials on graphene or reduced graphene oxide are

✉ Xiao Zhu
xzl412@126.com

1 School of Optical and Electronic Information, Huazhong University of Science and Technology, 1037 Luoyu Road, Wuhan 430074, P. R. China

vapor-phase and solution methods [4, 17, 23–25]. Compared to vapor-phase synthesis such as CVD, solution process is known as a route with the advantages of low-cost, low-temperature, large-scale manufacture and compatibility with flexible electronics. For the solution method, it is generally required to prepare ZnO seed layer by magnetron sputtering or high temperature annealing at the graphene surface to initiate the nucleation of ZnO. However, in the seeding process, the high temperature may lead to generate unintended defects in graphene, as well as be incompatible with flexible substrates. To avoid these problems, we used graphene oxide and crystallized ZnO nanocrystals nanocomposites as the seed layer to prepare GO/ZnO nanorods hybrids. In addition, the oxygen-containing groups (e.g., hydroxyl, carboxyl and epoxy groups) on the surface of graphene oxide could absorb the positively charged Zn^{2+} ions, and in turn provide nucleation and growth site by the reaction with OH^- ions, avoiding the usage of surfactant for compositing graphene and ZnO QDs [2].

In this study, a facile strategy is used to prepare GO/ZnO nanorods hybrid nanostructure UV detector with high sensitivity and fast-response by using GO/ZnO NCs as the seed layers. The effect of GO/ZnO NCs seed layer on the structure of ZnO nanorods is researched by field emission scanning electron microscope (FSEM) and its optical properties is studied by UV–Visible absorption. The introduction of GO in seed layer results in an ordered and uniformly aligned GO/ZnO nanorods array, thus, the absorbance and photocurrent increases significantly. The photocurrent of GO/ZnO nanorods can be improved almost one order of magnitude compared with pure ZnO nanorods. These results indicate that the addition of GO is contributed to the growth of ZnO nanorods and the improvement of photodetector performance.

2 Materials and methods

2.1 Synthesis of ZnO NCs

ZnO was prepared by a solvothermal method according to literature methods [19, 26]. Zinc acetate ($Zn(Ac)_2$, 4.46 mmol, 0.9791 g) was put into a flask containing 42 mL of methanol and the solution was stirred for 15 min. The PH of the solution was 6. Subsequently, the solution was heated to 60 °C with magnetic stirring. Potassium hydroxide (KOH, 7.22 mmol, 0.4264 g) was dissolved into 23 mL of methanol as the stock solution that was dropped into the flask within 4–6 min. The PH of the mixed solution was 8. Then, the mixed solution was kept at 60 °C for 2 h and 15 min with stirring. When the solution was cooled to room temperature and precipitated for 4 h, the upper solution was removed. Methanol (50 mL) was added to the solution and

stirred for 5 min. The upper solution was discarded again after 4 h. This process was repeated twice to wash the products by precipitation method. Finally, the obtained products were dispersed in a mixed solvent of chloroform and methanol (6 ml, 2:1 by volume) by ultrasonic for 5 min.

2.2 Preparation of GO/ZnO nanorods

Graphene oxide (GO) was purchase from Hengqiu Graphene Technology (Suzhou) Co.Ltd. 100 μL 2 mg mL^{-1} graphene oxide solution was added into 3 mL ZnO nanocrystal solution followed by magnetic stirring. Then 80 μL pure ZnO and GO/ZnO mixture solution were respectively spin-coated at 2000 rpm for 30 s on aluminum oxide substrates with Au electrodes (the distance was 300 μm), repeated this procedure to get a two-layered film. Subsequently, the samples were transfer to an beaker containing an aqueous solution of 0.025 M $Zn(Ac)_2$ (purity 99.99%, 0.219 g)/hexamethylenetetramine (HMT, purity 99%, 0.105 g, $(CH_2)_6N_4$). The volume of the aqueous solution was 40 mL. The nanorods were hydrothermally grown in the beakers at 95 °C for 0.5, 1, and 2 h respectively. After the completion of the reaction, the samples were rinsed with deionized water and blow-dried with ultra-high-purity (99.9999%) nitrogen to remove unreacted residual salts and organic materials. The whole process of preparing GO/ZnO nanorods was shown in Fig. 1.

2.3 Microstructure characterization

The crystallographic information of the obtained products was determined using an X-ray diffractometer (XRD, 7000S/L, Shimadzu Corp., Japan). The morphology observation was conducted using a field emission scanning electron microscope (FSEM, SU8010, Hitachi Corp., Japan) and transmission electron microscope (TEM, JME-2100(HR)). Raman scattering of the nanocomposite was collected on a Ranishaw in Via Raman microscope with an excitation laser of 532 nm. Absorption properties were investigated using a UV–Vis spectrometer with detecting range from 325 to 700 nm. Photodetector device performance was measured by Agilent (B1500A, America) inside an optically and electrically sealed box. Lighting was generated through a functional generator (Agilent 33210A) controlled 365 nm light-emitting diode.

3 Results and discussion

3.1 The characterizations of GO and ZnO NCs

We first studied the microstructure characterization of GO and ZnO. The XRD pattern of GO (Fig. 2a) displayed an
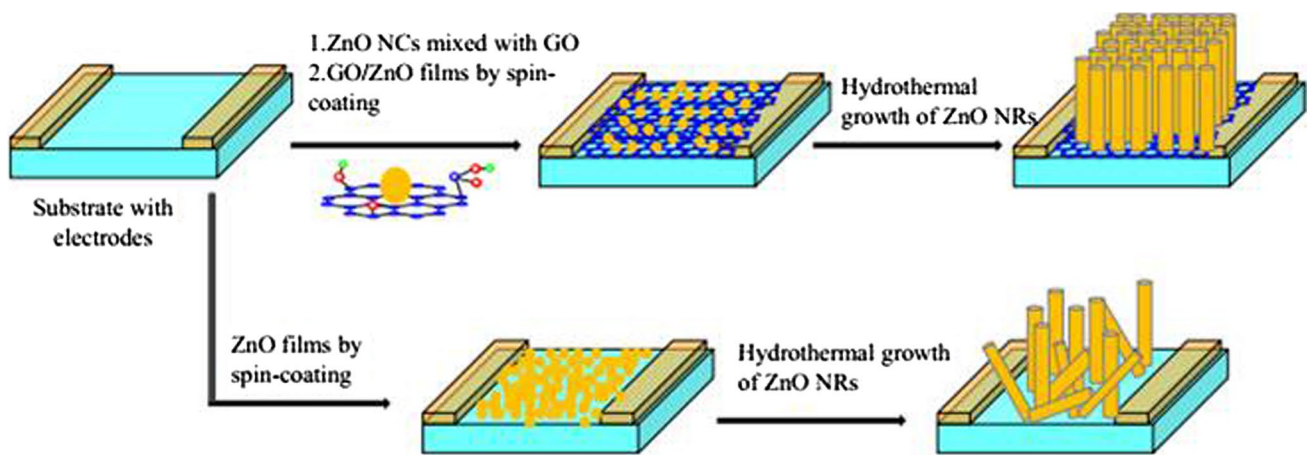
Fig. 1 Schematics of the GO/ZnO nanorods photodetector preparation
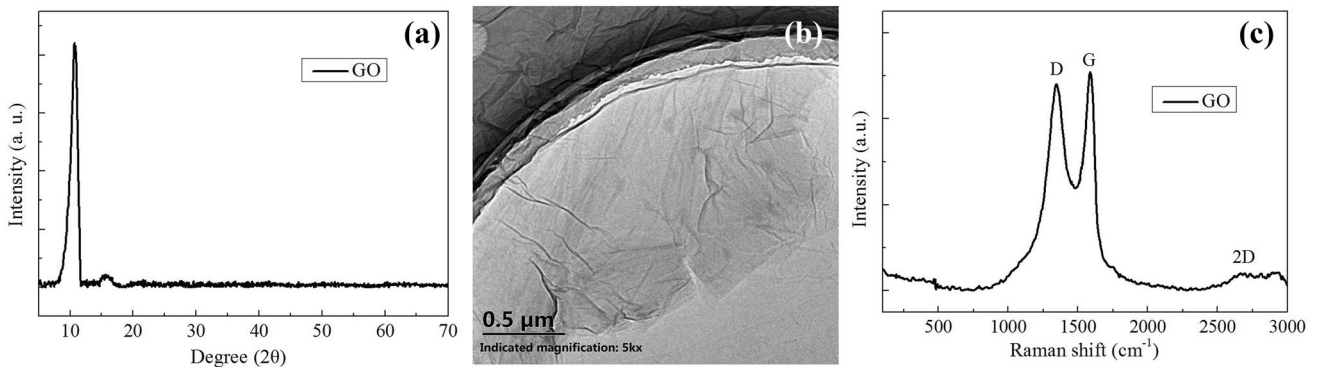

Fig. 2 Characterization of graphene oxide (GO). **a** XRD patterns of GO, **b** TEM micrograph of GO and **c** Raman spectrum of GO

intense and sharp diffraction at $2\theta = 10.8°$, which is attributed to the (001) lattice plane corresponding to a d-spacing of 0.82 nm, and this is consistent with the lamellar structure of GO. TEM (Fig. 2b) confirmed the high-quality graphene structure. Raman spectrum is commonly used to characterize graphite materials, especially to determine ordered and disordered crystal structures of graphene. The well-defined D and G bands of graphene can be observed in Raman spectra, as shown in Fig. 2c. The D and G bands were centered at approximately 1348 and 1590 cm^{-1}, respectively. The G band is attributed to the in-plane bond stretching of the C–C sp^2 bond, and the D band is associated with the various disorders and defects, such as vacancy-like defects and sp^3 defects [9, 14]. The intensity ratio of D to G band (I_D/I_G) in GO was 0.937, revealing numerous defects contained in the graphene oxide. In addition, the weak and broad 2D peaks appeared at approximately 2673 cm^{-1}, which was known as another indication of graphene sheets [27]. The microstructure characterizations of ZnO NCs were shown in Fig. 3. The XRD pattern (Fig. 3a) indicated that the ZnO NCs were formed with hexagonal wurtzite

structure [19, 28]. The TEM images (Fig. 3b, c) of ZnO NCs displayed that the average diameter of ZnO NCs was in the range of 6–9 nm.

Figure 4a, b shows the TEM images of GO/ZnO NCs nanocomposites, it can be seen that the ZnO nanocrystals tend to stack on the surface of GO while they were dispersed in the areas without GO, which indicated that ZnO nanocrystals were easy to attach onto the surface of graphene oxide due to the absorption effect between positively charged Zn^{2+} (chemisorbed on ZnO nanocryatals) and negatively charged surface of graphene oxide [2, 14]. The presence of GO and ZnO nanocrystals in the nanocomposites was further confirmed by X-ray diffraction (XRD). According to the XRD pattern (Fig. 3a), similar to the pure ZnO nanocrystals, the GO/ZnO nanocrystals hybrids exhibited six major characteristic diffraction peaks of hexagonal wurtzite structure ZnO. Meanwhile, the characteristic diffraction peaks of graphene oxide appeared at $2\theta \approx 10.8°$ in the GO/ZnO nanocrystals hybrids, which was consistent with the pristine graphene oxide. The result of TEM image and XRD pattern showed that ZnO nanocryatals were
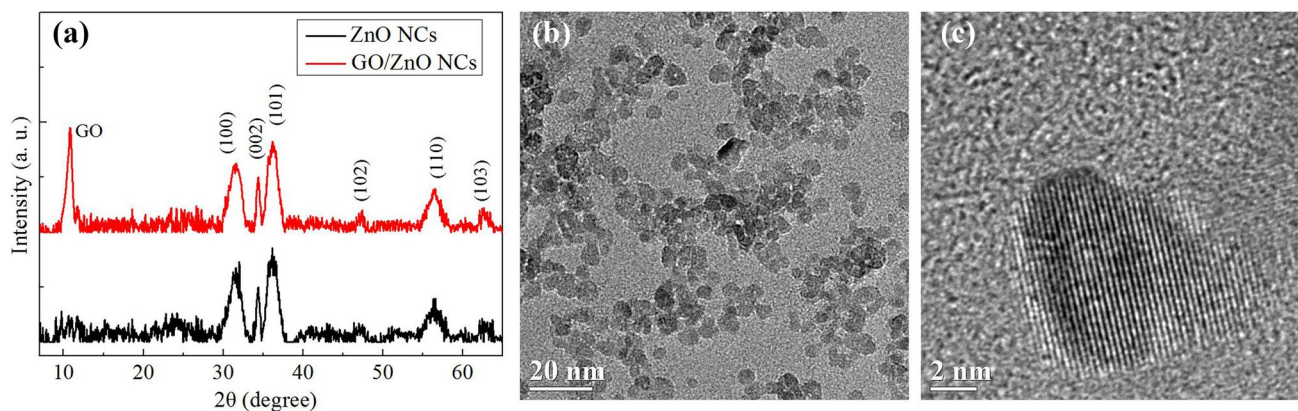
Fig. 3 a XRD pattern of ZnO and GO/ZnO nanocrystals, **b** TEM micrograph of ZnO nanocrystals and **c** HRTEM micrograph of single ZnO nanocrystal. (Color figure online)
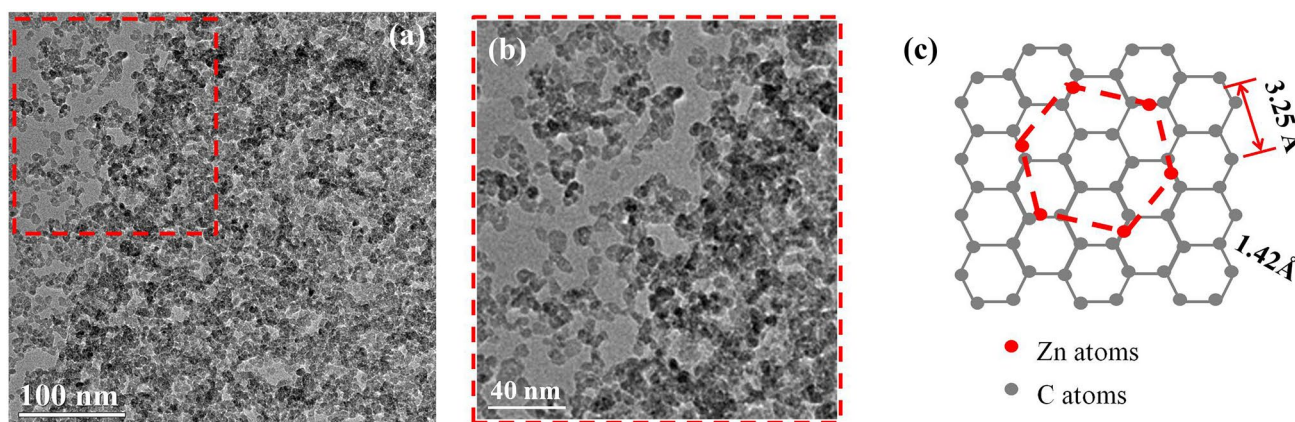

Fig. 4 a TEM micrograph of GO/ZnO NCs, **b** the magnified micrograph of (**a**) and **c** the epitaxial relationship between ZnO and graphene structure. (Color figure online)

easily distributed on the surface of GO, which would be helpful for the growth of ZnO nanorods on GO.

3.2 The characterizations of nanorods

XRD characterization was applied to measure ZnO nanorods and GO/ZnO nanorods grown for various time (Fig. 5). Both of ZnO nanorods and GO/ZnO nanorods showed diffraction peaks at $2\theta = 31.7°$, $34.4°$, $36.2°$, $47.6°$, $56.5°$ and $62.8°$, which could be indexed to the (100), (002), (101), (102), (110) and (103) lattice planes respectively. The sharp and narrow diffraction peaks indicated that the samples were well crystallized hexagonal wurtzite-type [13, 28]. Interestingly, the ZnO nanorods grown on GO/ZnO NCs seed layer showed a stronger diffraction peaks than that grown on ZnO NCs seed layer, which suggested that the addition of GO in seed layer was contributed to the growth and crystallization of ZnO nanorods. It may be that the oxygen-containing groups (such as hydroxyl,
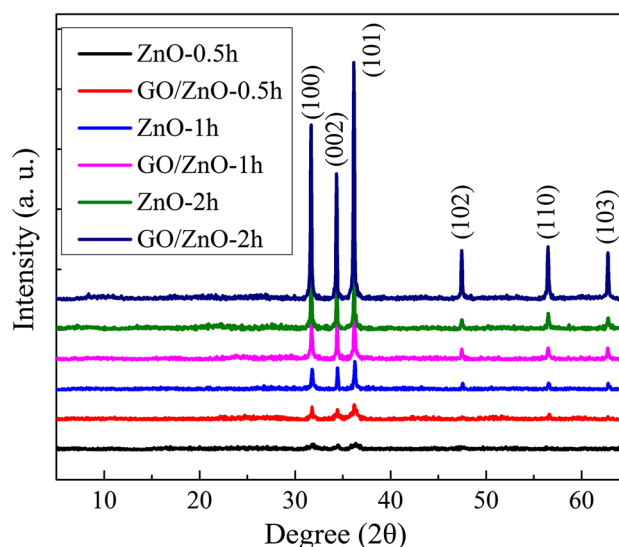

Fig. 5 XRD patterns of ZnO nanorods and GO/ZnO nanorods grown for various reaction time. (Color figure online)

carboxyl and epoxy groups) on GO absorbs the positively charged Zn^{2+}, and in turn provides ZnO growth sites by the reaction with OH^- ions [2, 14]. As a result, the growth of GO/ZnO nanorods was significantly enhanced compared to ZnO nanorods. In addition, with the increase of the growth time, the intensity of the diffraction peaks remarkably improved, which is understandable because extending the reaction time provides more opportunities for crystallization and growth of nanorods. However, the peaks from GO in the XRD pattern of the GO/ZnO nanorods were not detected, manifesting that the surface of the GO was completely covered with ZnO nanorods for all samples.

As shown in Fig. 6, the microstructures of various ZnO nanorods and GO/ZnO nanorods were measured and compared. It was found that the morphology of ZnO nanorods were related to the addition of GO in the seed layer. When the reaction time was 0.5 h, it could be clearly observed that dense ZnO nanorods were regularly distributed on GO/ZnO films (Fig. 6b) while sparse ZnO nanorods were disorderly distributed on ZnO films (Fig. 6a). This suggested that the addition of GO played an active role in the growth process of ZnO nanorods. ZnO NCs were easy to absorb on the surface of GO due to the presence of oxygen-containing groups (such as hydroxyl, carboxyl and epoxy groups), as shown in Fig. 4a [2, 14]. In the growth process of nanorods, ZnO NCs on GO acted as seeding sites to grow into nanorods. It is interesting to note that the lattice mismatch between the hexagonal ZnO crystal and graphene bond centered sites is very low (Fig. 4c). The length of C–C bond in graphene is ~1.42 Å, and the lattice constant c of wurtzite ZnO structure is ~3.25 Å, which is in accordance with the distance between two specific bond center, as shown in Fig. 4c [29]. This could lead to the like-epitaxial growth of ZnO nanorods on graphene structure [23, 29]. Since GO has the similar structure with graphene and there are only some oxygen-containing groups on the basal planes of graphene, it is likely for ZnO nanorods to like-epitaxial growth on GO. Therefore, the ZnO nanorods tend to grow perpendicular to the GO sheets [24, 29]. When pure ZnO NCs acted as the seeding sites, the absence of the like-epitaxial growth effect lead to random growth orientation. Thus, the GO/ZnO nanorods were better aligned than pure ZnO nanorods. In addition, various oxygen-containing groups on GO could provide new nucleation sites for the ZnO nanocrystal, which could realize a dense and compact growth for ZnO nanorods [2]. The diameter of the GO/ZnO nanorods was about 40 nm while the ZnO nanorods show a smaller diameter. With the increase of the reaction time, both of ZnO nanorods and GO/ZnO nanorods showed a dense and uniform distribution on the films, enough reaction time providing more opportunities for nucleation and growth. But it could be discerned that the orientation of GO/ZnO nanorods were still superior to ZnO nanorods and the diameter of GO/ZnO nanorods was still larger than that of ZnO nanorods. These results indicated that both of the introduction of GO in seed layer and extension of the reaction time were in favor of the growth and crystallization of ZnO nanorods, which was consistent with the XRD results.
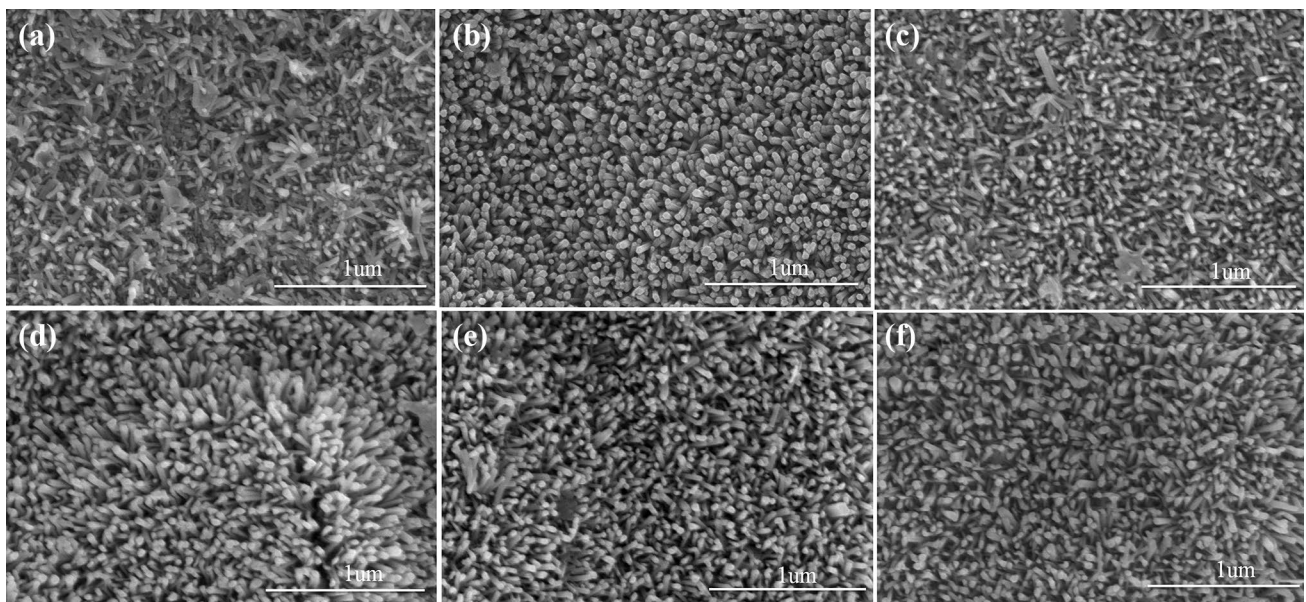

Fig. 6 FSEM images of various ZnO nanorods and GO/ZnO nanorods **a** ZnO—0.5 h, **b** GO/ZnO—0.5 h, **c** ZnO—1 h, **d** GO/ZnO—1 h, **e** ZnO—2 h and **f** GO/ZnO—2 h

3.3 UV–Vis absorption and photoresponse performance of nanorods

The UV–Visible absorption spectra of various ZnO nanorods and GO/ZnO nanorods were shown in Fig. 7. As can be seen, because of the quantum confinement effect, both of ZnO nanorods and GO/ZnO nanorods had a blue-shifted absorption peak at approximately 360 nm compared with that of bulk ZnO which had an absorption peak at 370 nm corresponding to a 3.35 eV bandgap at room temperature [30]. The absorbance of GO/ZnO nanorods was higher than that of ZnO nanorods, which may be due to the following reasons: firstly, there is an increase in surface electric charge of ZnO in the GO/ZnO nanorods due to the presence of GO, which may modify excition formation upon irradiation [13]; Secondly, the uniform and ordered GO/ZnO nanorods structures have less light scatting and stronger absorption of UV light compared to random structures [23, 31]. Therefore, the absorption rate of GO/ZnO nanorods is more outstanding.

Figure 8a presented the I–V curves taken from the GO/ZnO nanorods detector with the growth time of 1 h under different illuminating light intensities. The inset showed the current without irradiated with UV light. The dark current was recorded to be ~12 nA at 10 V bias. Upon UV illumination, the photoconductivity displayed a considerable increase. The photocurrent increased from 0.63 to 3.35 μA when the UV light power improved from 110 to 690 μW cm^{-2}. Stronger illumination gave rise to more light absorption rate and photo-generated carrier generation, meanwhile, higher voltage drove faster carrier circulation and more efficient carrier collection [32]. In order to investigate the kinetic behavior of photoresponses in more details, time-resolved photoresponses tests of GO/
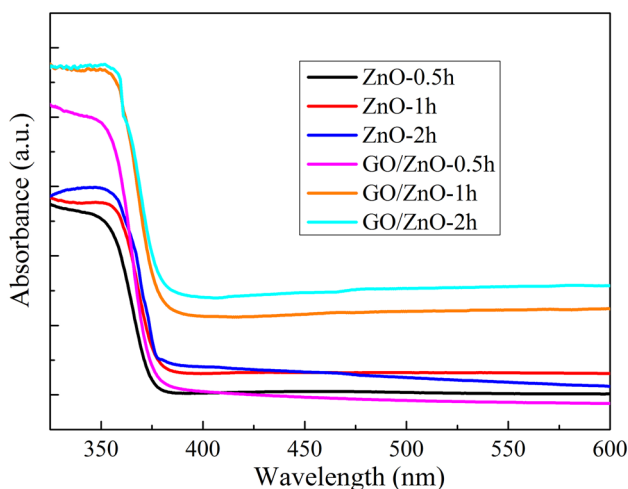

Fig. 7 UV–Vis spectra of ZnO nanorods and GO/ZnO nanorods grown for various reaction time. (Color figure online)

ZnO nanorods and pure ZnO nanorods were conducted at 10 V bias with 690 μW cm^{-2} illumination intensities, as shown in Fig. 8b–d. It can be seen that the generated photocurrent was significantly enhanced after the introduction of GO in the seed layer. When the growth time was 0.5 h, the photocurrent of GO/ZnO nanorods was 2.59 μA, which was much higher than that of the pure ZnO nanorods with 123 nA. Similarly, when the reaction time was 1 and 2 h, the photocurrents increased from 355 nA to 3.35 μA and from 614 nA to 3.39 μA respectively because of the existence of GO. Especially, when the reaction time was 1 h, the photocurrent of GO/ZnO nanorods was about 9.4 times larger than ZnO nanorods. This may be caused by two reasons. Firstly, the uniform and oriented GO/ZnO nanorods structures possess less light scatting and higher light absorption [31], which could be verified by the results of FSEM and UV–Visible spectrum, accordingly, the number of photo-generated carriers are enhanced. Secondly, the existence of GO effectively transmits the electrons from the ZnO nanorods to the surface of GO and inhibits the recombination of the photogenerated electron–hole pairs, resulting in longer carrier lifetime and hence higher photocurrent [12, 33]. Therefore, the GO/ZnO nanorods displayed better UV photoelectronic conversion properties compared to ZnO nanorods owing to the simultaneous improvement in light harvesting and charge transfer. Response current value are further used to evaluate the device parameters, namely responsivity (R_s) and detectivity (D^*). The R_s of device is defined as the ratio of the generated response current to the incident illumination power on the photodetector, which is given by $R_s = (I_{ph} - I_{dark})/P_oA$, where I_{ph} and I_{dark} are the current under illumination and in dark respectively, P_o is illumination power density and A is the effective device area (0.3×4 mm^2) [6, 34]. The calculated responsivity of pure ZnO nanorods device at 10 V bias was 42.59 mA W^{-1} while it increased to 403.04 mA W^{-1} for the GO/ZnO nanorods device when the reaction time was 1 h, which gives rise to prominent enhancement in the GO/ZnO nanorods device. This enhancement could be attribute to the enhanced light harvesting and charge transfer due to the influence of GO on the nanostructure and electron–hole pairs separation compared to pure ZnO nanorods device, as mentioned above. The detectivity (D^*) provides information about the noise of a photodetector. If we consider that the major contribution of noise is due to the dark current and then the detectivity can be given by [34]: $D^* = R_sA^{1/2}/(2qI_{dark})^{1/2}$, where q is an elementary charge. The unit of R_s, A, q and I_{dark} are A/W, cm^2, C and A respectively, thus, the unit of D^* is cm Hz$^{1/2}$ W^{-1} or Jones. The calculated detectivity of pure ZnO nanorods and GO/ZnO nanorods device for 1 h reaction time were 1.7×10^{11} and 7.17×10^{11} Jones, respectively. The higher detectivity of GO/ZnO nanorods device represents a higher
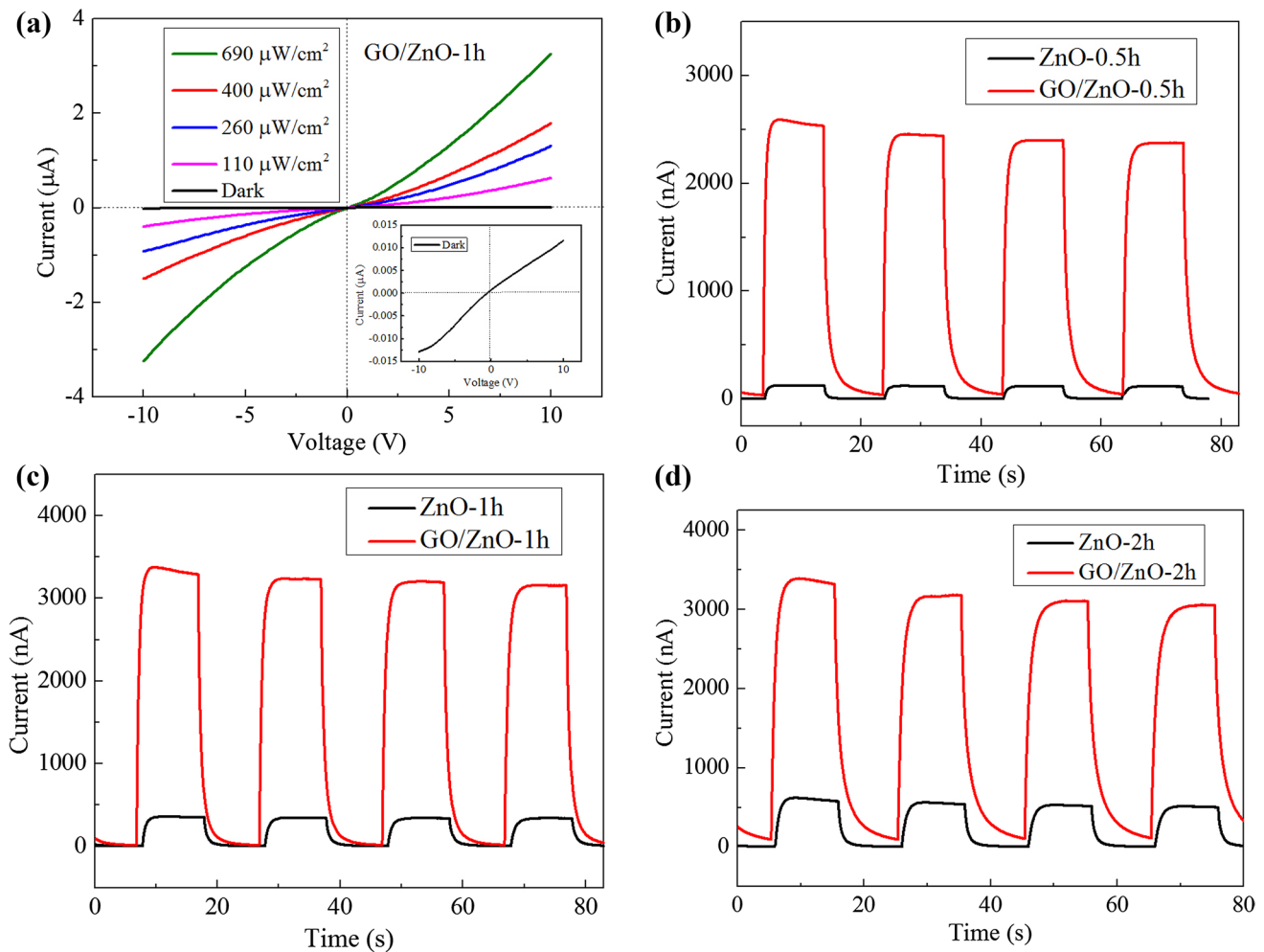
Fig. 8 **a** I–V characteristic curves of the GO/ZnO nanorods detector with the growth time of 1 h under different illuminating light intensities. I–t characteristic curves of ZnO nanorods and GO/ZnO nanorods with different growth time **b** 0.5 h, **c** 1 h and **d** 2 h. (Color figure online)

ability to detect small photosignals with low noise. In addition, response time can be defined as the time in which the photocurrent increases to 90% of its maximum value and recovery time can be defined as the time in which the photocurrent decrease to 10% of its maximum value, respectively. For GO/ZnO nanorods photodetector, the response time t_{90} was about 0.895 s and the recovery time t_{10} was around 1.536 s when the growth time was 1 h, which was not only faster than the ZnO nanorods device prepared in this study (response time t_{90} and recovery time t_{10} were 1.065 and 1.595 s respectively with reaction time being 1 h) but also much faster than many other ZnO nanostructures exhibited a response time range from decades of seconds to a few minutes [35]. It's worth noting that although the photoresponsivity of GO/ZnO nanorods being poorer than that of other UV photodetectors, the photocurrent increased significantly when the dark current was kept low and the response and recovery time are fast by utilizing this

simple method, and the results are summarized in Table 1. We believe that the method of introducing GO in the seed layer to prepare ZnO nanorods devices is a facile method to optimize the photoresponse properties of photodetector.

4 Conclusions

In summary, we employed a GO/ZnO NCs seed layer via a solvothermal method to prepare ZnO nanorods-based high performance UV photodetector. ZnO NCs was solution synthesized and then mixed with GO, the hybrids being spin-coated on substrate and acting as seed layer to prepare nanorods. Uniform and ordered ZnO nanorods arrays was formed with the introduction of GO, while the pure ZnO NCs seed layer yield sparse and randomly ZnO nanorods. Therefore, the GO/ZnO nanorods had enhanced light harvesting and improved photocurrent. The optimal

Table 1 The performance comparison of different ZnO based photodetectors

Photodetector	Bias (V)	I_{dark}	I_{ph}	R (A W^{-1})	t_{rise} (s)	t_{decay} (s)	Light (nm)	$L_{spacing\ gap}$	Ref.
ZnO nanorods /graphene	20	–	52.7 μA	22.7	>350	–	370	100 μm	[17]
ZnO nanorods	5	2.2 μA	28.3 μA	2.265	6.7	9.3	370	400 μm	[36]
ZnO nanowire/graphene foam	5	–	–	6	9.5	38	365	3 mm	[6]
ZnO nanowire	3	1.87 μA	2.36 mA	–	19.6	2.5	365	–	[37]
ZnO nanorod /graphene QDs	5	–	~0.5 mA	<0.75	>150	–	365	–	[38]
Graphene/ZnO nanowires	5	–	~3 mA	32000	11.9	240	365	90 μm	[34]
GO/ZnO nanorods (1 h)	10	11.8 nA	3.35 μA	0.403	0.895	1.536	365	300 μm	This work

photocurrent of GO/ZnO nanorods was 3.35 μA while the pure ZnO nanorods only showed a photocurrent of 355 nA. In addition, the response time t_{90} was about 0.895 s and the recovery time t_{10} was around 1.536 s for GO/ZnO nanorods photodetector, which was much faster than the pure ZnO nanorods photodetector. Therefore, the introduction of GO into seed layer played an active role in the structure and photoresponse properties of nanorods, and the method of using GO/ZnO NCs as the seed layer via low-temperature solvothermal process provided a simple and low-cost technical to fabricate high performance ZnO based photodetector, which could be extend to other material systems for practical application.

References

1. A.M. Bazargan, F. Sharif, S. Mazinani, N. Naderi, J. Mater. Sci. **27**, 8221 (2016)
2. D.I. Son, B.W. Kwon, D.H. Park, W.S. Seo, Y. Yi, B. Angadi, C.L. Lee, W.K. Choi, Nat. Nanotechnol. **7**, 465 (2012)
3. M. Norouzi, M. Kolahdouz, P. Ebrahimi, M. Ganjian, R. Soleimanzadeh, K. Narimani, H. Radamson, Thin Solid Films **619**, 41 (2016)
4. Q. Xu, Q.J. Cheng, J.X. Zhong, W.W. Cai, Z.F. Zhang, Z.Y. Wu, F.Y. Zhang, Nanotechnology **25**, 055501 (2014)
5. R. Slama, J. El Ghoul, I. Ghiloufi, K. Omri, L. El Mir, A. Houas, J. Mater. Sci. **27**, 8146 (2016)
6. B.D. Boruah, A. Mukherjee, S. Sridhar, A. Misra, ACS Appl. Mater. Interfaces **7**, 10606 (2015)
7. M.K. Kavitha, P. Gopinath, H. John, Phys. Chem. Chem. Phys. **17**, 14647 (2015)
8. S.M. Hatch, J. Briscoe, A. Sapelkin, W.P. Gillin, J.B. Gilchrist, M.P. Ryan, S. Heutz, S. Dunn, J. Appl. Phys. **113**, 204501 (2013)
9. H. Liu, Q. Sun, J. Xing, Z.Y. Zheng, Z.L. Zhang, Z.Q. Lü, K. Zhao, ACS Appl. Mater. Interfaces **7**, 6645 (2015)
10. R.R. Nair, P. Blake, A.N. Grigorenko, K.S. Novoselov, T.J. Booth, T. Stauber, N.M.R. Peres, A.K. Geim, Science **320**, 1308 (2008)
11. S.M. Chen, M. Gao, L. Zhao, Z.Q. Ma, J. Mater. Sci. **26**, 6961 (2015)
12. X.B. Liu, H.J. Du, X.W. Sun, RSC Adv. **4**, 5136 (2014)
13. M.K. Kavitha, H. John, P. Gopinath, R. Philip, J. Mater. Chem. C **1**, 3669 (2013)
14. M. Sookhakian, Y.M. Amin, R. Zakaria, W.J. Basirun, M.R. Mahmoudian, B. Nasiri-Tabrizi, S. Baradaran, M. Azarang, J. Alloys Compd. **632**, 201 (2015)
15. X.C. He, C.X. Zhang, J.H. Pi, Z.Z. Wang, H. Wei, J. Mater. Sci. **26**, 1853 (2015)
16. Q.L. Bao, K.P. Loh, ACS Nano **6**, 3677 (2012)
17. H.X. Chang, Z.H. Sun, K.Y.F. Ho, X.M. Tao, F. Yan, W.M. Kwok, Z.J. Zheng, Nanoscale **3**, 258 (2011)
18. F.N. Xia, T. Mueller, Y.M. Lin, A.V. Garcia, P. Avouris, Nat. Nanotechnol. **4**, 839 (2009)
19. Z.Y. Zhan, L.X. Zheng, Y.Z. Pan, G.Z. Sun, L. Li, J. Mater. Chem. **22**, 2589 (2012)
20. D.L. Shao, M.P. Yu, H.T. Sun, T. Hu, J. Lian, S. Sawyer, Nanoscale **5**, 3664 (2013)
21. J.Q. Yu, J. Jin, B. Cheng, M. Jaroniec, J. Mater. Chem. A **2**, 3407 (2014)
22. S. Ratha, A.J. Simbeck, D.J. Late, S.K. Nayak, C.S. Rout, Appl. Phys. Lett. **105**, 243502 (2014)
23. R.K. Biroju, N. Tilak, G. Rajender, S. Dhara, P.K. Giri, Nanotechnology **26**, 145601 (2015)
24. X.J. Men, H.B. Chen, K.W. Chang, X.F. Fang, C.F. Wu, W.P. Qin, S.Y. Yin, Appl. Catal. B **187**, 367 (2016)
25. G. Nam, J.Y. Leem, RSC Adv. **5**, 94222 (2015)
26. B.Q. Sun, H. Sirringhaus, Nano Lett. **5**, 2408 (2005)
27. S. Safa, R. Sarraf-Mamoory, R. Azimirad, J. Sol–gel Sci. Technol. **74**, 499 (2015)
28. K. Anand, O. Singh, R.C. Singh, Appl. Phys. A **116**, 1141 (2014)
29. M. Yu, Y. Ma, J. Liu, X. Li, S. Li, S. Liu, Appl. Surf. Sci. **390**, 266 (2016)
30. Y.Z. Jin, J.P. Wang, B.Q. Sun, J.C. Blakesley, N.C. Greenham, Nano Lett. **8**, 1649 (2008)
31. G. Wang, D. Chen, H. Zhang, J.Z. Zhang, J.H. Li, J. Phys. Chem. C **112**, 8850 (2008)
32. J. He, M. Luo, L. Hu, Y. Zhou, S. Jiang, H. Song, R. Ye, J. Chen, L. Gao, J. Tang, J. Alloys Compd. **596**, 73 (2014)
33. M. Azarang, A. Shuhaini, R. Yousefi, M. Sookhakian, J. Appl. Phys. **116**, 084307 (2014)
34. B.D. Boruah, D.B. Ferry, A. Mukherjee, A. Misra, Nanotechnology **26**, 235703 (2015)
35. Z.X. Wang, X.Y. Zhan, Y.J. Wang, S. Muhammad, Y. Huang, J. He, Nanoscale **4**, 2678 (2012)
36. O.F. Farhat, M.M. Halim, M.J. Abdullah, M.K.M. Ali, N.M. Ahmed, N.K. Allam, Appl. Phys. A **119**, 1197 (2015)
37. L. Ren, T.T. Tian, Y.Z. Li, J.G. Huang, X.J. Zhao, ACS Appl. Mater. Interfaces **5**, 5861 (2013)
38. B. Yang, J. Chen, L. Cui, W. Liu, RSC Adv. **73**, 59204 (2015)